[7]Lancaster, P., *Lambda Matrices and Vibrating Systems*, Pergamon, Oxford, 1966, p. 127.

A. Berman
Associate Editor

Dispersion Relations in Piezoelectric Coupled Beams

Q. Wang* and S. T. Quek†
National University of Singapore, Singapore 119260, Republic of Singapore

I. Introduction

ONE of the main reasons for the recent popularity of the use of piezoelectric materials as both actuator and sensor is their versatility and efficiency in transforming mechanical energy to electrical energy and vice versa. Basic mechanics models for the interaction of beams, coupled with piezoelectric actuators and sensors, either surface bonded on or embedded in the host beam structure, have been proposed by several researchers.[1–4] Crawley and de Luis[3] developed a uniform strain model for a beam with surface-bonded and embedded piezoelectric actuator patches. Crawley and Anderson[5] later deduced the mechanics model for the coupled structure based on an Euler beam assumption of the displacement field. Leibowitz and Vinson[6] provided a general model in which the elastic layers, soft-core layers, or piezoelectric layers are included by using the Hamilton principle. These models commonly assumed a linear distribution for the electric potential in the transverse direction, which inevitably violates Maxwell's electric equation. To overcome this, Krommer and Irschik[7] suggested a parabolic distribution, whereas Lee and Lin[8] assumed a full-cycle sine distribution for the electric potential in wave propagation problems in plate structures. Wave propagation in uncoupled beams has long been studied, where dispersion relations based on Euler, Rayleigh, Timoshenko, and exact theories have been presented.[9]

The objective of this Note is to present results of dispersion wave propagation curves for beams with surface-bonded piezoelectric players. The qualitative effect of the coupled piezoelectric materials on wave propagation in beams studied herein will serve as a reference for further analyses of wave propagation in piezoelectric coupled structures. Two models of beam theory are explored, namely, Euler and Timoshenko.[10] Both models assume that plane sections remain plane, but in Euler beam theory the sections remain perpendicular to the neutral axis. This assumption is removed in Timoshenko beam theory[10] to account for the effect of shear. The dispersion curves for different thickness ratios between the piezoelectric layer and host beam structure are obtained by assuming a half-cycle cosine potential distribution in the transverse direction of the piezoelectric material. In addition, the phase velocity for wave number approaching infinity and the cutoff frequencies based on the Timoshenko beam model are also presented.

II. Electric Fields in the Coupled Beam

Figure 1 shows the layout of a surface-mounted piezoelectric coupled beam with total thickness $2h$. The width is assumed to be unity for convenience, without loss of generality. Each piezoelectric layer has a thickness of h_1 and has an electrode mounted on the external surface for applying external electric voltage to actuate the structure. When an external electric voltage is applied, the electric potential distribution on the surface of the electrode remains constant.

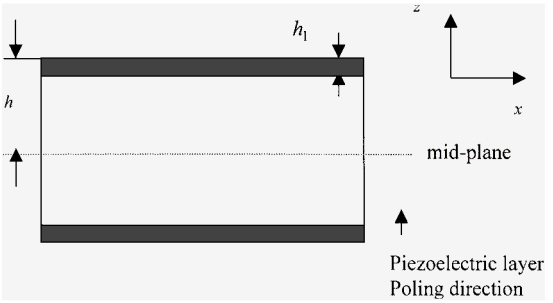

Fig. 1 Beam structure with surface-mounted piezoelectric layers.

When electrodes at the two surfaces of the piezoelectric layer are connected, the electric potential is zero throughout the surfaces. As stated earlier, most recent published papers assumed a constant electric field across the thickness of the piezoelectric material and a uniform distribution of the electric potential in the longitudinal direction. By the assuming of sinusoidal electric potential distribution in the transverse z direction, not only is Maxwell's static electricity equation not violated, but the corresponding distribution of the electric potential in the longitudinal direction can be solved.[11] In this Note, a half-cycle cosine distribution for the electric potential in the transverse z direction is assumed, which is more appropriate for beam vibration in the flexural mode.[7] For the general case, the potential function, assuming a combined cosine and linear variation of electric potential in the transverse z direction, can be written as

$$\phi = \phi(x, z, t) = -\cos(\pi z_l / h_1) \cdot \bar{\phi}(x) e^{i\omega t} + (2z_1 / h_1)\phi_a e^{i\omega t} \tag{1a}$$

where z_l is measured from the center of the piezoelectric layer in the global z direction, h_1 is the thickness of the layer, $\bar{\phi}(x)$ is the spatial variation of the electric potential in the global x direction, and ϕ_a is the value of external electric voltage applied to the electrodes. From Eq. (1a), we can see that the electric potentials at the two surfaces of the piezoelectric layer, that is, $z_1 = \pm h_1$, are exactly the electric voltage $\pm\phi_a$ applied to the electrodes. When there is no external electric voltage applied to the electrodes, the electric potentials at the surfaces of the layer are zero, which can be seen clearly from Eq. (1a). Because this Note addresses only wave propagation analysis, Eq. (1a) can be simplified as

$$\phi = -\cos(\pi z_l / h_1) \cdot \bar{\phi}(x) e^{i\omega t} \tag{1b}$$

in which the distribution function $\bar{\phi}(x)$ will be obtained from the coupling equation derived hereafter.

The spatial amplitude of the electric field $\bar{E}$ and electric displacement $\bar{D}$ are then written as

$$\bar{E}_x = \cos\frac{\pi z_l}{h_1} \cdot \frac{\partial \bar{\phi}}{\partial x} \tag{2}$$

$$\bar{E}_z = \frac{\pi}{h_1} \sin\frac{\pi z_l}{h_1} \bar{\phi} \tag{3}$$

$$\bar{D}_x = \Xi_{11} \bar{E}_x \tag{4}$$

$$\bar{D}_z = \Xi_{33} \bar{E}_z + E_p d_{31} \bar{\varepsilon}_x \tag{5}$$

where Ξ_{11}, $\bar{E}_x$, Ξ_{33}, and $\bar{E}_z$ are the dielectric constant and electric field of the piezoelectric layer in the x and z directions, respectively; $\bar{D}_x$ and $\bar{D}_z$ are the corresponding electric displacements; E_p is the Young's modulus of the piezoelectric layer in its longitudinal x direction; and d_{31} is the piezoelectric strain coefficient. Next, the displacement field for the two beam models will be discussed.

III. Wave Propagation Based on Euler Beam Model

For a long and thin beam, Euler theory is usually assumed, and the displacement field can be expressed as

$$u_z = \bar{u}(x) e^{i\omega t} \tag{6}$$

$$u_x = -z \frac{\partial \bar{u}(x)}{\partial x} e^{i\omega t} \tag{7}$$

Received 11 March 2000; revision received 25 July 2000; accepted for publication 21 August 2000.

*Assistant Professor, Civil Engineering Department, 10 Kent Ridge Crescent; cvewangq@nus.edu.sg.

†Associate Professor, Civil Engineering Department, 10 Kent Ridge Crescent.

where u_z and u_x are the displacements in the transverse z direction and longitudinal x direction of the beam, respectively, and ω is the natural frequency of the beam. Note that $\bar{u}(x)$ must satisfy the mechanical boundary conditions, which are specific to each problem. For example, $\bar{u}(x)$ and its second derivative at the boundary are all zero for a simply supported boundary condition.

The poling direction of the piezoelectric material is assumed to be in the direction of the transverse displacement of the beam. When voltages of equal magnitude but opposite sign are applied to the upper and lower piezoelectric layers of the beam, a differential strain is induced, resulting in bending of the beam. The amplitude of the strain ε and stress σ in the beam and piezoelectric layer may be deduced accordingly as

$$\bar{\varepsilon}_x = -z\frac{\partial^2 \bar{u}}{\partial x^2} \tag{8}$$

$$\bar{\sigma}_x^1 = -Ez\frac{\partial^2 \bar{u}}{\partial x^2} \tag{9}$$

$$\bar{\sigma}_x^2 = -E_p z\frac{\partial^2 \bar{u}}{\partial x^2} - E_p d_{31} E_z \tag{10}$$

where the superscripts 1 and 2 represent the variables in the beam and piezoelectric material, respectively; the overbar denotes the spatial part of the dynamic variable; and E is Young's modulus of the beam material.

The moment caused by the stresses is expressed, in view of Eqs. (3), (9), and (10), as

$$M_x = 2\left(\int_0^{h-h_1} z\bar{\sigma}_x^1\,\mathrm{d}z + \int_{h-h_1}^{h} z\bar{\sigma}_x^2\,\mathrm{d}z\right) = -A_1\bar{\phi} - B_1\frac{\partial^2 \bar{u}}{\partial x^2} \tag{11}$$

where

$$A_1 = -2E_p d_{31}\frac{\pi}{h_1}\int_{h-h_1}^{h} z\sin\frac{\pi(z-h+h_1/2)}{h_1}\,\mathrm{d}z = -\frac{4E_p d_{31}h_1}{\pi} \tag{12}$$

$$\begin{aligned} B_1 &= 2\left[E\int_0^{h-h_1} z^2\,\mathrm{d}z + E_p\int_{h-h_1}^{h} z^2\,\mathrm{d}z\right] \\ &= \frac{2}{3}\Big[E\left(h^3 - 3hh_1^2 + 3h^2h_1 - h_1^3\right) \\ &\quad + E_p\left(3hh_1^2 - 3h^2h_1 + h_1^3\right)\Big] \end{aligned} \tag{13}$$

Substituting Eq. (11) into the Euler beam equilibrium equation,

$$\rho A\frac{\partial^2 u}{\partial t^2} = \frac{\partial^2 M}{\partial x^2}$$

gives

$$A_1\frac{\partial^2 \bar{\phi}}{\partial x^2} + B_1\frac{\partial^4 \bar{u}}{\partial x^4} + [\rho(2h-2h_1) + 2\bar{\rho}h_1](-\omega^2)\bar{u} = 0 \tag{14}$$

From the Maxwell equation,

$$\int_{h-h_1}^{h} \nabla\bar{D}\,\mathrm{d}z = 0$$

and in view of Eqs. (4) and (5), we have

$$C_1\frac{\partial^2 \bar{\phi}}{\partial x^2} + D_1\bar{\phi} + E_1\frac{\partial^2 \bar{u}}{\partial x^2} = 0 \tag{15}$$

where

$$C_1 = \Xi_{11}\int_{h-h_1}^{h} \cos\frac{\pi(z-h+h_1/2)}{h_1}\,\mathrm{d}z = \frac{2\Xi_{11}h_1}{\pi} \tag{16}$$

$$D_1 = -\Xi_{33}\left(\frac{\pi}{h_1}\right)^2\int_{h-h_1}^{h} \cos\frac{\pi(z-b-h_1/2)}{h_1}\,\mathrm{d}z = -\frac{2\Xi_{33}\pi}{h_1} \tag{17}$$

$$E_1 = -E_p d_{31}\int_{h-h_1}^{h} \mathrm{d}z = -E_p d_{31}h_1 \tag{18}$$

For wave propagation in an infinite beam, the solutions are assumed to take the following form:

$$u(x,t) = Ue^{i(\gamma x-\omega t)} \tag{19a}$$

$$\phi(x,t) = \Phi e^{i(\gamma x-\omega t)} \tag{19b}$$

Introducing Eq. (19) into Eqs. (14) and (15) yields

$$-\gamma^2 A_1\Phi + \left\{B_1\gamma^4 - \omega^2[\rho(2h-2h_1) + 2\bar{\rho}h_1]\right\}U = 0 \tag{20a}$$

$$-C_1\gamma^2\Phi + D_1\Phi - E_1\gamma^2 U = 0 \tag{20b}$$

From Eq. (20b),

$$\Phi = \frac{E_1\gamma^2}{D_1 - C_1\gamma^2}U \tag{21}$$

and the resulting relation between frequency and wave number is

$$-\frac{A_1E_1\gamma^4}{D_1 - C_1\gamma^2} + B_1\gamma^4 - \omega^2\left[\rho(2h-2h_1) + 2\bar{\rho}h_1\right] = 0 \tag{22}$$

By the substitution of $\omega = c\gamma$, the relation between phase velocity and wave number is obtained:

$$-\frac{A_1E_1\gamma^2}{D_1 - C_1\gamma^2} + B_1\gamma^2 - c^2\left[\rho(2h-2h_1) + 2\bar{\rho}h_1\right] = 0 \tag{23}$$

Using the nondimensional expressions $\gamma = \bar{\gamma}/h$ and $c = \bar{c}\sqrt{(E/\rho)}$, we have the phase velocity as

$$\begin{aligned} \bar{c} &= \bar{\gamma}\sqrt{-\frac{A_1E_1}{D_1h^2 - C_1\bar{\gamma}^2} + \frac{B_1}{h^2}\Bigg/\left[E\left(2h-2h_1+\frac{2\bar{\rho}h_1}{\rho}\right)\right]} \\ &= \bar{\gamma}\sqrt{\frac{2E_p^2d_{31}^2r^3}{\Xi_{33}\pi + \Xi_{11}r^2\bar{\gamma}^2} + \frac{2}{3}\left[E(1-r)^3 + E_p(3r-3r^2+r^3)\right]\Bigg/\left[E\left(2-2r+\frac{2\bar{\rho}}{\rho}r\right)\right]} \end{aligned} \tag{24}$$

where $r = h_1/h$. With the material properties of the host structure and piezoelectric layer shown in Table 1, the dispersion curves (nondimensional phase velocity against nondimensional wave number) are plotted in Fig. 2 for $r = 0$, 0.1, 0.2, 0.3, and 0.4. The result shows that the phase velocity/wave number relationship in a piezoelectric coupled beam is virtually linear with the slope decreasing as h_1 increases. The difference when the piezoelectric layer is considered and omitted is not negligible.

IV. Wave Propagation Based on Timoshenko Beam Model[10]

In the Euler beam model, the effects of rotary inertia and shear deformation are neglected. In 1894, Rayleigh[12] corrected for the effect of rotary inertia. Subsequently, Timoshenko[10] included both effects of shear and rotary inertia and obtained results of wave propagation in better agreement with those using exact theory. A new variable φ is introduced to measure the slope of the cross section due to bending, and the displacement and strain field in the x direction is modified as

$$u_x = -z\bar{\varphi}(x)e^{i\omega t} \tag{25}$$

$$\bar{\varepsilon}_x = -z\frac{\partial\bar{\varphi}(x)}{\partial x} \tag{26}$$

The corresponding stress components are written as

$$\bar{\sigma}_x^1 = -Ez\frac{\partial\bar{\varphi}(x)}{\partial x} \tag{27}$$

$$\bar{\sigma}_x^2 = -E_p z\frac{\partial\bar{\varphi}(x)}{\partial x} - E_p d_{31}E_z \tag{28}$$

Given the same electrical potential distribution as in the Euler beam model, the components of moment and shear force are obtained as

$$M_x = 2\left(\int_0^{h-h_1} z\bar{\sigma}_x^1\,\mathrm{d}z + \int_{h-h_1}^{h} z\bar{\sigma}_x^2\,\mathrm{d}z\right) = -A_1\bar{\phi} - B_1\frac{\partial\bar{\varphi}}{\partial x} \tag{29}$$

$$V = (AG)_c\kappa\left[\frac{\partial\bar{u}(x)}{\partial x} - \bar{\varphi}(x)\right] \tag{30}$$

Table 1 Material properties ($\Xi_0 = 8.854 \times 10^{-12}$ F/m)

Parameter	Host structure	Piezoelectric layer
Height, m	0.01	——
Young's modulus E_p, N/m^2	78.0×10^9	69.0×10^9
Poisson's ratio	0.29	0.35
Mass density, kg/m^3	7.8×10^3	7.4×10^3
d_{31}, C/N	——	-179×10^{-12}
Ξ_{11}/Ξ_0	——	200
Ξ_{33}/Ξ_0	——	195

where $(GA)_c = G_h(2h - 2h_1) + 2G_p h_1$, $G_h = [E/2(1 + \upsilon)]$ is the shear modulus of the host structure, $G_p = [E_p/2(1 + \bar{\upsilon})]$ the shear modulus of piezoelectric layer, where $\bar{\upsilon}$ is Poisson's ratio of the piezoelectric layer, and κ is the shear effect that is taken as 0.833 for a rectangular cross section.

The governing equations using Timoshenko beam model are given as[10]

$$\frac{\partial V}{\partial x} + q = (\rho A)_c\frac{\partial^2 u}{\partial t^2} \tag{31}$$

$$V - \frac{\partial M_x}{\partial x} = (\rho I)_c\frac{\partial^2\varphi}{\partial t^2} \tag{32}$$

where $(\rho A)_c = \rho(2h - 2h_1) + 2\bar{\rho}h_1$ and $(\rho I)_c = \frac{2}{3}\rho(h - h_1)^3 + \frac{2}{3}\bar{\rho}\left[h^3 - (h - h_1)^3\right]$.

When wave propagation is considered in an infinite Timoshenko beam,[10] the expression for φ is given as

$$\varphi = \Psi e^{i(\gamma x - \omega t)} \tag{33}$$

Substituting Eqs. (29), (30), and (33) into Eqs. (31) and (32) gives

$$(GA)_c\kappa\left(\frac{\partial\bar{\varphi}}{\partial x} - \frac{\partial^2\bar{u}}{\partial x^2}\right) - (\rho A)_c\omega^2\bar{u} = 0 \tag{34}$$

$$(GA)_c\kappa\left(\frac{\partial\bar{u}}{\partial x} - \bar{\varphi}\right) + B_1\frac{\partial^2\bar{\varphi}}{\partial x^2} + A_1\frac{\partial\bar{\phi}}{\partial x} + (\rho I)_c\omega^2\bar{\varphi} = 0 \tag{35}$$

The Maxwell equation remains similar to Eq. (15), except for the last term.

Substituting Eqs. (19) and (33) into Eqs. (15), (34), and (55), we have

$$\left[(GA)_c\kappa\gamma^2 - (\rho A)_c\omega^2\right]U + i(GA)_c\kappa\gamma\Psi = 0 \tag{36}$$

$$i(GA)_c\kappa\gamma U - \left[(GA)_c\kappa + B_1\gamma^2 - (\rho I)_c\omega^2\right]\Psi + iA_1\gamma\Phi = 0 \tag{37}$$

$$-\gamma^2 C_1\Phi + D_1\Phi + iE_1\gamma\Psi = 0 \tag{38}$$

Equation (38) leads to

$$\Phi = \frac{-E_1 i\gamma}{D_1 - C_1\gamma^2}\Psi \tag{39}$$

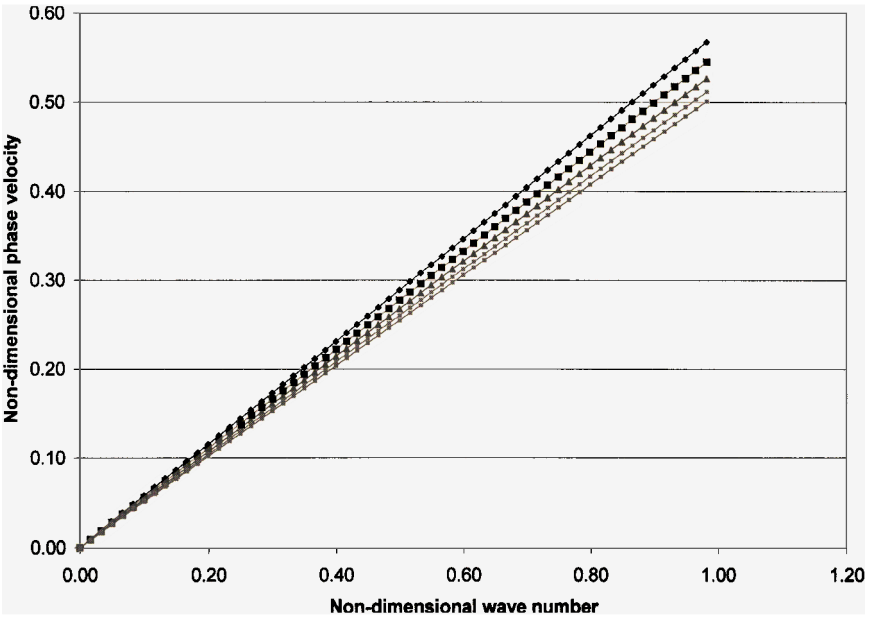

Fig. 2 Dispersive curves in Euler beam model: ◆, $r = 0$; ■, $r = 0.1$; ▲, $r = 0.2$; ■, $r = 0.3$; and ■, $r = 0.4$.

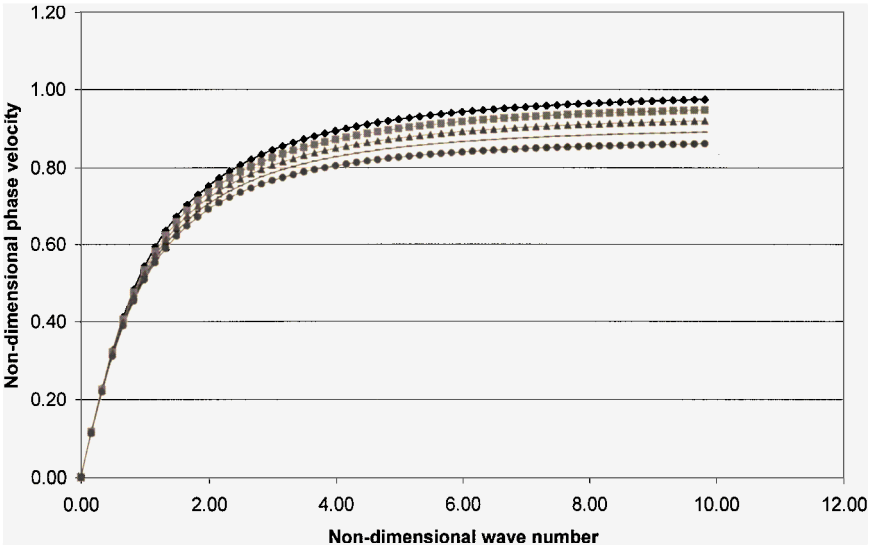

Fig. 3 Dispersive curves in Timoshenko beam model: ◆, $r = 0$; ■, $r = 0.1$; ▲, $r = 0.2$; ——, $r = 0.3$; and ●, $r = 0.4$.

and Eq. (37) becomes

$$i(GA)_c \kappa \gamma U - \left[(GA)_c \kappa + B_1 \gamma^2 - \frac{E_1 A_1 \gamma^2}{D_1 - C_1 \gamma^2} - (\rho I)_c \omega^2 \right] \Psi = 0 \quad (40)$$

By the substitution of $\omega = c\gamma$, the relation between phase velocity and wave number is obtained by combining Eqs. (36) and (40) as

$$\frac{(\rho I)_c}{(GA)_c \kappa} c^4 - \left\{ \frac{1}{\gamma^2} + \frac{(\rho I)_c}{(\rho A)_c} + \frac{B_1 - \left[E_1 A_1 \middle/ \left(D_1 - C_1 \gamma^2 \right) \right]}{(GA)_c \kappa} \right\} c^2 + \frac{B_1 - \left[E_1 A_1 \middle/ \left(D_1 - C_1 \gamma^2 \right) \right]}{(\rho A)_c} = 0 \quad (41)$$

With the nondimensional expressions $\gamma = \bar{\gamma}/h$ and $c = \bar{c}\sqrt{(G\kappa/\rho)}$, the phase velocity is obtained as

$$\bar{c} = \sqrt{\frac{Y - \sqrt{Y^2 - 4XZ}}{2X}} \left(\frac{\rho}{G\kappa} \right)^{\frac{1}{2}} \quad (42)$$

where

$$Y = \frac{1}{h^{-2}\bar{\gamma}^2} + \frac{(\rho I)_c}{(\rho A)_c} + \frac{B_1 - \left[E_1 A_1 \middle/ (D_1 - C_1 h^{-2} \bar{\gamma}^2) \right]}{(GA)_c \kappa} \quad (43)$$

$$X = \frac{(\rho I)_c}{(GA)_c \kappa} \quad (44)$$

$$Z = \frac{B_1 - \left[E_1 A_1 \middle/ \left(D_1 - C_1 h^{-2} \bar{\gamma}^2 \right) \right]}{(\rho A)_c} \quad (45)$$

With the same materials as in Table 1, the dispersion curves are plotted in Fig. 3. Consistent with Fig. 2, the phase velocity decreases as h_1 increases for a given wave number. With larger wave number, the phase velocity/wave number relationship deviates from linearity, consistent with that of an uncoupled beam. The piezoelectric effect based on the Timoshenko model[10] is also significant.

To study the asymptotic behavior as the wave number becomes large, Eq. (41) reduces to

$$\lim_{\gamma \to \infty} \bar{c} = \sqrt{\frac{\bar{Y} - \sqrt{\bar{Y}^2 - 4X\bar{Z}}}{2X}} \left(\frac{\rho}{G\kappa} \right)^{\frac{1}{2}} \quad (46)$$

where

$$\bar{Y} = \frac{(\rho I)_c}{(\rho A)_c} + \frac{B_1}{(GA)_c \kappa} \quad (47a)$$

$$\bar{Z} = \frac{B_1}{(\rho A)_c} \quad (47b)$$

Consistent with the results of Kolsky,[9] the wave velocities are bounded at large wave numbers, in contrast to that from the Euler model. The long-wavelength limit ($\gamma \to 0$) can also be investigated for the possibility of cutoff frequencies. That is,

$$\omega_{c1} = 0 \quad (48a)$$

$$\omega_{c2} = \sqrt{\frac{(GA)_c \kappa}{(\rho I)_c}} \quad (48b)$$

V. Summary

It is shown in this Note that the effect of the piezoelectric materials on the dispersion properties of a beam can be significant based on both Euler and Timoshenko[10] theory. From the numerical simulations with the materials in Table 1, we can see that, for a given wave number, the phase velocity decreases as thicker piezoelectric materials are used. The asymptotic behavior based on the Timoshenko beam model is presented where the cutoff frequency is a function of the ratio between the shear and flexural rigidity. The coupled piezoelectric effects are analyzed by assuming a half-cycle cosine distribution for the electric potential in the transverse direction of the beam and imposing a Maxwell equation. The results of this Note can serve as a reference for future study of wave propagation in coupled plates as well as in the design of ultrasonic motors incorporating piezoelectric materials.

Acknowledgment

The work in this Note is supported by a Research Grant from the National University of Singapore, R-264-000-057-112.

References

[1] Bailey, T., and Hubbard, J. E., Jr., "Distributed Piezoelectric Polymer Active Vibration Control of a Cantilever Beam," *Journal of Guidance, Control, and Dynamics*, Vol. 8, 1985, pp. 605–611.

[2] Lee, C. K., "Theory of Laminate Piezoelectric Plates for the Design of Distributed Sensors/Actuators, Part 1: Governing Equations and Reciprocal Relationships," *Journal of the Acoustical Society of America*, Vol. 87, 1990, pp. 1144–1158.

[3] Crawley, E. F., and de Luis, J., "Use of Piezoelectric Actuators as Elements of Intelligent Structures," *AIAA Journal*, Vol. 25, 1987, pp. 1373–1385.

[4] Wang, B. T., and Rogers, C. A., "Laminate Plate Theory for Spatially Distributed Induced Strain Actuators," *Journal of Composite Materials*, Vol. 25, 1991, pp. 433–452.

[5] Crawley, E. F., and Anderson, E. H., "Detailed Model of Piezoelectric Actuation of Beams," *Proceedings of the 30th AIAA/ASME/SAE Structures,*

Structural Dynamics, and Materials Conference, AIAA, Washington, DC, 1989, pp. 2000–2010.

[6]Leibowitz, M., and Vinson, J. R., "The Use of Hamilton's Principle in Laminated Piezoelectric and Composite Structures," *Adaptive Structures and Material Systems*, AD-35, 1993, pp. 257–267.

[7]Krommer, M., and Irschik, H., "On the Influence of the Electric Field on Free Transverse Vibrations of Smart Beams," *Smart Materials and Structures*, Vol. 8, 1999, pp. 401–410.

[8]Lee, P. C. Y., and Lin, W. S., "Piezoelectrically Forced Vibrations of Rectangular SC-Cut Quartz Plates," *Journal of Applied Physics*, Vol. 83, 1998, pp. 7822–7833.

[9]Kolsky, H., *Stress Waves in Solids*, Dover, New York, 1963.

[10]Timoshenko, S. P., "On the Correction for Shear of the Differential Equation for Transverse Vibrations of Prismatic Bars," *Philosophical Magazine*, Vol. 41, 1921, pp. 744–746.

[11]Wang, Q., and Quek, S. T., "Flexural Vibration Analysis of Sandwich Beam Coupled with Piezoelectric Actuator," *Smart Materials and Structures*, Vol. 9, 2000, pp. 103–109.

[12]Rayleigh, J. W. S., *The Theory of Sound*, Vols. 1 and 2, Dover, New York, 1945.

A. M. Waas
Associate Editor

Buckling and Postbuckling of Compressible Circular Rings Under Hydrostatic Pressure

John V. Huddleston* and M. V. Sivaselvan†
State University of New York at Buffalo, Buffalo, New York 14260-4300

I. Introduction

IT is important for the designer of ribbed undersea vessels to understand how the buckling and postbuckling behavior of rings under external pressure is affected by two factors: 1) the shape of the ring and 2) the centerline extensibility or compressibility of the ring. In this Note, the simplest case of a circular ring with uniform cross section is studied. The method of solution used can also be applied to rings pressurized internally, such as those in aircraft or space structures. That, however, is a simpler problem to solve because there is no bifurcation point in the response of such rings. Still, the two mentioned factors also affect the response of those rings.

Figure 1 shows a circular, compressible ring subjected to a uniform external pressure p per unit length of deformed centerline (which we use because of the way hydrostatic pressure behaves physically). Such a ring will deform into a smaller circle as the pressure is increased, until a bifurcation point is reached, and then it will buckle into a noncircular shape. Figure 2 shows three possible buckled configurations. In Fig. 2a, the deformed centerline has two axes of symmetry, and integration is required from point A to point B only. In Fig. 2b, the deformed shape has only one axis of symmetry, requiring integration from A to C. Finally, in Fig. 2c, there is no symmetry, and the integration must be carried out from A all the way around and back to point A.

The only problems previously solved in the literature have assumed that the ring has uniform cross-sectional area A and uniform moment of inertia I along its centerline, and only the doubly symmetric mode of buckling has been considered. The method used in the present Note is not restricted to uniform section properties. These may vary along the centerline. Then, if the original circle has only the x axis as an axis of symmetry with respect to the section properties, the buckled shape might also be singly symmetric, in which case Fig. 2b would apply. If the original circle lacked any symmetry whatever in the section properties, then Fig. 2c would apply. The present Note, however, deals only with the doubly symmetric mode. It shows how the buckling and postbuckling behavior of symmetrical circular rings is affected by the axial compressibility of the ring.

Previous recent work on problems similar to this has been done by Wang[1] and Fu and Waas.[2] Because the ring in Wang's[1] problem contained a hinge at point C, he had to assume a singly symmetric deformed configuration similar to that in Fig. 2b. The results obtained, however, were limited to incompressible rings. Fu and Waas[2] considered thick rings, as we do in the present Note, but their results were limited to the initial postbuckling stage. Our method permits analysis of the entire postbuckling regime.

The buckling of rings under hydrostatic, constantly directed, and centrally directed pressure using classical energy approaches is discussed by El Naschie.[3] His book is also a source of references to earlier works on circular rings.

II. Theory

Table 1 shows the nonlinear boundary-value problem that describes the buckled ring for the case of doubly symmetric deformation (as well as describing the compressed circular ring before the critical pressure is reached). The equations in Table 1 are taken from the work of Huddleston[4] and are not restricted to slender rings except insofar as the underlying assumption that plane sections remain plane ultimately limits the thickness of the ring. It is difficult to say at what thickness our results are appreciably affected by this limitation because shear deformations enter the picture for thick rings and shear deformations in curved members are not well understood. The notation in Table 1 is as follows:

s_0	=	distance along original centerline measured from point A
θ	=	angle of inclination of final centerline at each point
ξ	=	final x coordinate of general point
η	=	final y coordinate of general point
s	=	distance along final centerline measured from point A
K_0	=	original curvature of centerline
N	=	normal force at general cross section
M	=	bending moment at general cross section
E	=	Young's modulus
A	=	cross-sectional area
I'	=	section property, defined by

$$\iint_A \frac{y^2}{1 - K_0 y}\,\mathrm{d}A$$

where the y in this integral is a coordinate from the centroidal axis of the cross section to the general point on the cross section.

Actually, the differential equations in Table 1 are not restricted to circular rings. They apply to rings of any original shape, as long as the original curvature at each point along the centerline is used during the integration process.

Because of the need to find N and M at each point during the integration, the four geometric differential equations in Table 1 must

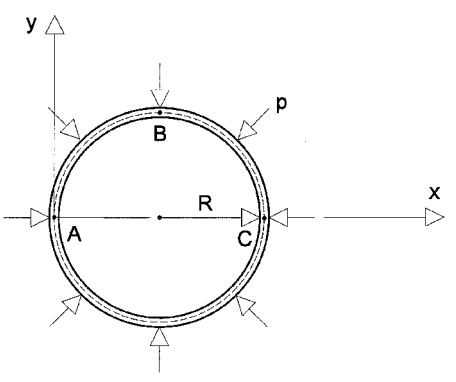

Fig. 1 Compressible circular ring under hydrostatic pressure.

Received 23 February 2000; revision received 15 August 2000; accepted for publication 21 August 2000.

*Professor of Engineering and Applied Sciences, Emeritus, Department of Civil, Structural, and Environmental Engineering.

†Graduate Student, Department of Civil, Structural, and Environmental Engineering.